Amino Acids (2015) 47:543–559
DOI 10.1007/s00726-014-1887-8

ORIGINAL ARTICLE

Structural analysis of membrane-bound hECE-1 dimer using molecular modeling techniques: insights into conformational changes and $A\beta_{1-42}$ peptide binding

Kailas D. Sonawane · Sagar H. Barage

Received: 14 May 2014 / Accepted: 28 November 2014 / Published online: 16 December 2014

Abstract The human endothelin converting enzyme-1 (hECE-1) is a homodimer linked by a single disulfide bridge and has been identified as an important target for Alzheimer's disease. Structural analysis of hECE-1 dimer could lead to design specific and effective therapies against Alzheimer's disease. Hence, in the present study homology model of transmembrane helix has been constructed and patched with available crystal structure of hECE-1 monomer. Then, membrane-bound whole model of hECE-1 dimer has been developed by considering biophysical properties of membrane proteins. The explicit molecular dynamics simulation revealed that the hECE-1 dimer exhibits conformational restrains and controls total central cavity by regulating the degree of fluctuations in some residues (238–226) for substrate/product entrance/exit sites. In turn, conformational rearrangements of interdomain linkers as well as helices close to the inner surface are responsible for increasing total central cavity of hECE-1 dimer. Further, the model of hECE-1 dimer was docked with $A\beta_{1-42}$ followed by MD simulation to investigate possible orientation and interactions of $A\beta_{1-42}$ in catalytic groove of hECE-1 dimer. The free energy calculations exposed the stability of complex and helped us to identify key residues of hECE-1 involved in interactions with $A\beta_{1-42}$ peptide. Hence, the present study might be useful to understand structural significance of membrane-bound dimeric hECE-1 to design therapies against Alzheimer's disease.

Keywords Human endothelin converting enzyme (hECE-1) · Homology modeling · MD simulation · Molecular docking · $A\beta_{1-42}$ peptide

Introduction

Human endothelin converting enzyme-1 (hECE-1) is a type II integral membrane protein expressed by endothelial cells of aorta, lungs, ovary and testis (Ahn et al. 1992; Takahashi et al. 1993; Ohnaka et al. 1993; Takahashi et al. 1995). The hECE-1 has four isoforms (ECE-1a–d) derived from same gene and shows more activity at neutral pH (Schweizer et al. 1997; Valdenaire et al. 1999b; Hans-Dieter et al. 1997). These four human ECE-1 isoforms, termed as ECE-1a (758 residues), ECE-1b (770 residues), ECE-1c (754 residues) and ECE-1d (767 residues), resemble similar catalytic properties but distinct subcellular localization and tissue distribution (Schweizer et al. 1997; Valdenaire et al. 1999a). The Cysteine 412 and 428 contribute to form dimeric structure of ECE-1 in rat and human, respectively (Shimada et al. 1996; Schulz et al. 2009).

ECE-1 is a key enzyme involved in biosynthesis pathway of endothelins (Xu et al. 1994). Endothelin (ET) is the most powerful vasoconstrictor produced by vascular endothelial cells by action of endothelin converting enzyme (Yanagisawa et al. 1988; Inoue et al. 1989). The inhibition of endothelin converting enzyme is an intuitive approach to reduce elevated plasma ET-1 concentration associated with cardiovascular diseases (Krum et al. 1998; Kedzeirski

Electronic supplementary material The online version of this article (doi:10.1007/s00726-014-1887-8) contains supplementary material, which is available to authorized users.

K. D. Sonawane (✉)
Structural Bioinformatics Unit, Department of Biochemistry, Shivaji University, Kolhapur 416 004, Maharashtra, India
e-mail: kds_biochem@unishivaji.ac.in

S. H. Barage
Department of Biotechnology, Shivaji University, Kolhapur 416 004, Maharashtra, India

et al. 2001; Kirkby et al. 2008). The cell-based and in vitro assays demonstrate that hECE-1 has been implicated in the Aβ peptide degradation (Eckman et al. 2001). The involvement of hECE-1 has also been shown to degrade Aβ peptides at physiological conditions and hence, considered as a therapeutic target in Alzheimer's disease (Eckman et al. 2005; Miners et al. 2011; Eckman et al. 2001; Barage and Sonawane 2014; Barage et al. 2014). Besides this, it has also been found that ECE-1 isoforms (ECE-1a and ECE-1c) provide an evidence for non-catalytic roles in promoting and suppressing prostate cancer cell invasion, mediated through their unique N-terminal regions (Lambert et al. 2008). Thus, ECE-1 is also a relevant target for anti-invasive therapy in prostate and other cancers (Lambert et al. 2008).

The hECE-1 is composed of three domains including short N-terminal cytoplasmic domain, followed by a single transmembrane helix, and larger C-terminal extracellular domain containing active site residues. The four isoforms differ only in the cytoplasmic and transmembrane domain whereas extracellular C-terminal domains are identical (Xu et al. 1994; Turner and Tanzawa 1997). The crystal structure of the extracellular domain (residues 100–770) of hECE-1 complexed with phosphoramidon has been solved using X-ray crystallography at 2.38 Å resolution (Schulz et al. 2009). The monomeric C412S mutant of rat ECE-1 (C428S in human) has been shown to have much lower affinity for substrate and inhibitor as compared to the wild-type ECE-1 dimer (Shimada et al. 1996). Moreover, monomeric ECE-1 has much lower efficiency for the cleavage of big ET-1 as well as minimal activity against small substrates like Leu-enkephalin (Johnson et al. 1999). Because of the difficulties encountered in the crystallization of membrane proteins, homology modeling is being served as a valuable technique to generate reliable 3D models (Hillisch et al. 2004; Tseng et al. 2007; Cavasotto and Phatak 2009). Therefore, understanding of extracellular substrate activities of hECE-1 remains a challenge due to the lack of appropriate structural information. All these studies highlight that structural information of this enzyme will be essential to understand the mechanism of action and to guide hECE-1-based therapies in the treatment of Alzheimer's disease. But three-dimensional structural arrangement of membrane-bound disulfide-linked hECE-1 dimer has not been solved at atomic level.

Hence, we built homology model of 10 missing residues and transmembrane helices of hECE-1 to understand the differences in catalytic rates of monomeric and dimeric enzymes. Subsequently, MD simulation of hECE-1 dimer embedded in lipid bilayer was performed to understand its flexibility and dynamic behavior. Detailed analysis of secondary structural elements revealed that dynamic conformational changes are found around the active site residues and on the surface of hECE-1 dimer. Such conformational changes at hECE-1 surface are beneficial to the entrance/exit of substrate/product. Furthermore, the molecular docking of $A\beta_{1-42}$ followed by MD simulation was carried out to investigate binding modes of $A\beta_{1-42}$ peptide and key residues of hECE-1 implicated in the stabilization of enzyme substrate complex. These results support that substrate/product could enter or exit from the observed cavity mouths at the surface of hECE-1. The present study might be useful to clarify the differences in catalytic rates of monomeric and dimeric forms as well as restricted substrate specificity of hECE-1.

Materials and methods

Homology modeling of hECE-1

The crystal structure of hECE-1 complexed with inhibitor phosphoramidon was used as a starting structure (PDB ID: 3DWB). It represents an extracellular domain (residues 100–770) of monomeric hECE-1 mutant C428S with 10 missing residues (^{422}YGTKKTCLPR^{431}) (Schulz et al. 2009). These residues are involved in the dimerization process (Schulz et al. 2009; Shimada et al. 1996). The hECE-1 crystal structure is patched with these missing residues as per previous modeling criteria (Tseng et al. 2007; Barage and Sonawane 2014). Subsequently, model of N-terminal domain with single transmembrane helix was built using homology modeling technique. The complete amino acid sequence of N-terminal domain with transmembrane helix of hECE-1 consisting of 100 residues was retrieved from UniProt protein sequence database (UniProt entry P42892). The secondary structure prediction programs like SOPMA (Geourjon and Deleage 1995) and GOR (Garnier et al. 1996) were used to obtain structural pattern of the protein sequence in terms of helix, sheets and coils. Along with this, the transmembrane prediction servers such as TMHMM (Krogh et al. 2001) and PredictProtein (Rost et al. 2004) have been applied to identify the location of transmembrane helix, intracellular loops (ICLs), and extracellular loops (ECLs) of whole hECE-1.

The sequence of N-terminal domain with transmembrane helix (100 residues) has been used to search suitable template against structural database (PDB) with the help of NCBI's PSI-BLAST programme (Altschul et al. 1997). The default search algorithm parameters of PSI-BLAST were changed to obtain relevant template for N-terminal domain modeling. The crystal structure of *S. cerevisiae* Exo70 (PDB: 2PFV.pdb; Moore et al. 2007) was used as a template to construct models of transmembrane region of hECE-1. Using information of primary and secondary structures, the final alignment between target and template

was edited manually using BioEdit (version 7.0.9.0) (Hall 1999) to retain high equivalence of conserved regions. Then three-dimensional model of N-terminal domain with transmembrane helix was generated using MODELLER 9v7 (Sali and Blundell 1993; Khemili et al. 2012). Similarly, for comparison we have also built a homology model of N-terminal domain with transmembrane helix using MUSTER (MUlti-Source ThreadER) program (Wu and Zhang 2008). The stereochemical quality assessment methods such as PROCHECK (Laskowski et al. 1993) and ProSA-web (*Z*-scores) (Wiederstein and Sippl 2007) were used to check the reliability of generated model. Structural comparison has also been made between template and generated model of N-terminal domain structure using PDBeFOLD programme (Krissinel and Henrick 2004). The generated model of N-terminal domain with transmembrane helix has been connected to whole hECE-1 crystal structure using UCSF chimera (Pettersen et al. 2004). All bond length, bond angle and dihedral angle values were set to its proper position to construct a whole hECE-1 model. Modeling criteria were maintained similarly as used in the earlier studies (Tseng et al. 2007; Barage and Sonawane 2014).

Membrane-bound hECE-1 dimer preparation

The generated monomer of hECE-1b is composed of N-terminal cytoplasmic domain, followed by a single transmembrane helix and C-terminal extracellular domain contains active site residues (Schulz et al. 2009; Bur et al. 2001). A copy of hECE-1b monomer was made and manually translated and rotated in such a way that the two bridging residues cysteines 428 of each hECE-1b monomer come closer to minimal distance to form disulfide bond without forming repulsive interactions with other parts of enzyme (Bur et al. 2001). The make bond option was used to generate disulfide bond between cysteine 428 of two monomers using UCSF chimera (Pettersen et al. 2004). The generated hECE-1 dimer was subjected to energy minimization using GROMACS 4.5.5 program (Pronk et al. 2013) to remove strain energy. The hECE-1 dimer is then oriented in such a way that transmembrane helix is aligned with non-polar lipid tails using GROMACS tool *editconf* by applying translation and rotational vectors only to the protein (Wallin et al. 1997; Pronk et al. 2013). The previously equilibrated palmitoyloleoylphosphatidylethanolamine (POPE) lipid bilayer and lipid parameters were obtained from P. Tieleman's site at http://moose.bio.ucalgary.ca (Tieleman and Berendsen 1998). The transmembrane helix of hECE-1 dimer was inserted into the lipid bilayer, while C-terminal domain exposed outside of bilayer using the InflateGro program (Kandt et al. 2007; Faraldo-Gomez et al. 2002). Each compression step was followed by energy minimization with steepest descent method to relax lipid molecules by keeping protein restrained. The overlapping lipid molecules are removed on the basis of simple distance cutoff between the TM helix and lipid molecule as per previous computational studies (Henin et al. 2005; Kandt et al. 2007). Finally, hECE-1 dimer embedded in lipid bilayer consists of 334 lipid molecules.

Molecular dynamics simulation of hECE-1 dimer with lipid bilayer

The MD simulation study of the hECE-1 dimer embedded in a POPE lipid bilayer was performed using GROMACS 4.5.5 program with force field parameters employed in previous studies (Poger et al. 2010; Poger and Mark 2010). The partial atomic charge on zinc ion and coordinating atoms was assigned as per previous computational studies (Pelmenschikov et al. 2002; Grossman et al. 2011; Barage and Sonawane 2014). The entire system was then solvated with simple point charge (SPC) water model and neutralized with Na^+ counter ions. The solvated structure was then minimized by steepest descent energy minimization method. The energy minimization was followed by 500 ps equilibration in the NVT ensemble with position restraints applied to protein. Subsequently, system was equilibrated for 2 ns using NPT ensemble. The final production run was performed up to 50 ns at 310 K temperature and 1 bar pressure under isothermal–isobaric (NPT) ensemble. Nosé–Hoover temperature (which is used widely for membrane NPT simulations) and Parrinello–Rahman pressure coupling methods were used to maintain temperature and pressure values. The protein, lipids and water including ions were coupled separately to a temperature bath with a coupling constant of $\tau t = 0.1$ ps. Semi-isotropic pressure coupling was set with $\tau p = 1$ ps, allowing the bilayer to deform in the *x*–*y* plane independently of the *z*-axis. Since the interfacial system like membrane–water system has a tendency to move laterally, the motion of the bilayer center-of-mass (COM) and solvent COM was reset separately so that the overall COM for the system is unchanged as the phases may drift in opposite directions. A time step of 2 fs was used throughout with periodic boundary conditions. The LINCS algorithm (Hess 2008) was used to constrain bond length to maintain the geometry of molecule and van der Waals interactions were evaluated using 1.2 nm cutoff distance. The long range electrostatic interactions were calculated using PME algorithm (Essmann et al. 1995). All simulations were performed on IBM Blade server HS22 having 64 Intel Xeon 2.53 GHz Hexa Core processors. The areas and volumes of pockets located on the protein surface as well as the void buried in the protein interior were calculated using an alpha shape-based pocket method from CASTp server (Dundas et al. 2006). The CAVER 3.0 tool was employed to delineate the shape of the main tunnel

and the slot connecting the active site with the bulk solvent (Chovancova et al. 2012). The trajectory was analyzed using VMD software (Humphrey et al. 1996). Simulation images were generated using chimera (Pettersen et al. 2004) and PyMOL (http://pymol.sourceforge.net/).

Molecular docking of hECE-1 dimer and $A\beta_{1-42}$ peptide

Molecular docking has been performed between final MD simulated structure of hECE-1 dimer and amyloid beta ($A\beta_{1-42}$) peptide. The Kollman united atom charges were assigned to receptor hECE-1 atoms similar to our earlier studies (Barage and Sonawane 2014; Barage et al. 2014; Dhanavade et al. 2013; Jalkute et al. 2013). The active site amino acid residues, zinc ion interacting residue charges and protonation states were assigned properly as per earlier studies (Hu and Shelver 2003; Irwin et al. 2005). The zinc parameters such as radius, well depth and charges were given as per earlier report (Hu and Shelver 2003; Irwin et al. 2005). Three-dimensional structure of $A\beta_{1-42}$ peptide (PDB: 1IYT.pdb) was used as a ligand molecule and then minimized by steepest descent method to remove steric clashes from the initial structure similar to earlier study (Crescenzi et al. 2002; Dhanavade and Sonawane 2014). The minimized structure of Aβ peptide was docked with hECE-1 using AutoDock 4.2 (Morris et al. 2009). Lamarckian genetic algorithm (LGA) has been used in this study. The grid map was set to 82 × 82 × 82 points with a grid spacing of 0.25 Å centered on the substrate binding channel of hECE-1 composed of S1, S1′ and S2′ subsites and zinc binding site (Morris et al. 2009; Barage and Sonawane, 2014; Papakyriakou et al. 2007). The grid box contains the entire binding site of the hECE-1 and provides enough space to Aβ peptide for translation and rotation. Step size of 0.25 Å for translation and 5° for rotation was chosen and a maximum number of energy evaluations were set to 2.5×10^6. Thus, 100 runs were carried out. For 100 independent runs, a maximum number of 27,000 GA operations were generated on a single population of 100 individuals. The generated docked conformations were ranked by predicted binding energy. The best docked conformation was selected based on different citeria including orientation of Aβ peptide and its residue side chain properly accomodated in the active site of hECE-1. The selected complex of hECE-1 and $A\beta_{1-42}$ peptide was subjected to 5 ns MD simulation with similar methodology as described in the previous section. Similarly, we have also docked other $A\beta_{1-40}$ peptide conformation extracted from 1AML.pdb (Sticht et al. 1995) and 1BA4.pdb (Coles et al. 1998) with hECE-1 dimer. However, these docked complexes show highest binding energies and were not considered for MD simulation.

Binding free energy calculations of hECE-1 and $A\beta_{1-42}$ peptide complex

The Molecular Mechanics/Poisson–Boltzmann Surface Area (MM/PBSA) method was used to calculate binding free energies of macromolecules as described previously (Hou et al. 2011; Spiliotopoulos et al. 2012). For this purpose, 25 snapshots of complex (hECE-1 and $A\beta_{1-42}$) were chosen evenly from 0 to 5 ns MD trajectories as per earlier report (Hou et al. 2011; Genheden and Ryde, 2010). The same snapshot has been used to calculate different energetic parameters using MM/PBSA method (Vorontsov and Miyashita 2011; Hou et al. 2011; Genheden and Ryde 2010). The binding interaction of each receptor (hECE-1) and ligand ($A\beta_{1-42}$) residue pairs was calculated in three terms such as van der Waals contribution (ΔE_{vdw}), electrostatic contribution (ΔE_{ele}), and solvation contribution (ΔE_{sol}).

Results and discussion

Homology modeling of hECE-1

The monomer of hECE-1b is composed of N-terminal cytoplasmic domain (1–50), followed by a single transmembrane helix (69–91) and C-terminal extracellular domain (100–770) contains active site residues as depicted in Table S1. Secondary structural analysis of residues was present in N-terminal domain with transmembrane helix of hECE-1b sequence (UniProt entry P42892) performed using SOPMA (Geourjon and Deleage 1995). This analysis revealed that 47, 8, 7 and 38 % amino acid residues are present in helices, extended strands, turns and random coils respectively, while GOR (Garnier et al. 1996) program shows that 53, 8 and 39 % amino acid residues are present in helices, strands and random coils respectively (Fig. S1). The overall secondary structure analysis showed that hECE-1 exhibits structural conservation of single transmembrane helix which plays an important role in the attachment of extracellular domain to the membrane as explained earlier (Xu et al. 1994; Shimada et al. 1996).

The homology modeling of membrane protein is quite difficult because of the lack of experimentally determined structures and the low sequence similarity with available structure (Hillisch et al. 2004). PSI-BLAST (Altschul et al. 1997) programme has been employed to obtain distant homolog of membrane part. The crystal structure of *S. cerevisiae* Exo70 (PDB: 2PFV.pdb) (Moore et al. 2007) showed 31 % similarity with 100 residues of transmembrane helix region of hECE-1b. A prerequisite for homology modeling is an accurate sequence alignment between target and template. Therefore, the final alignment between hECE-1 and

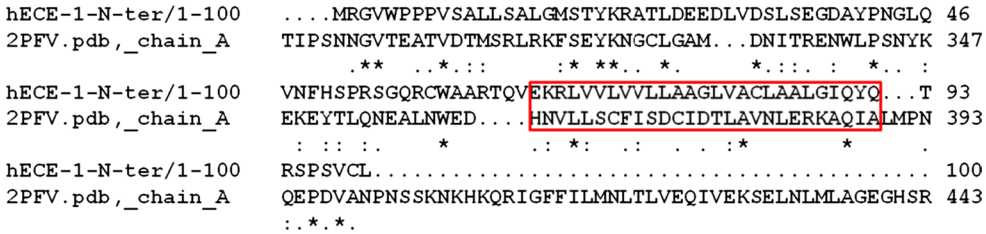

Fig. 1 Pairwise sequence alignment of N-terminal domain and transmembrane helix (100 residues) with template (2PFV). Transmembrane helix is indicated by *red outlined box* (color figure online)

2PFV.pdb was edited using BioEdit (Hall 1999). Based on final alignment (Fig. 1) 50 models were generated with MODELLER 9v7 standard parameters (Sali and Blundell 1993; Khemili et al. 2012). All generated models were energy minimized to remove strain energy. Among them, the single model was selected on the basis of GA341 and Discrete Optimized Protein Energy (DOPE) scoring functions available with MODELLER (Shen and Sali 2006).

The PROCHECK analysis of the hECE-1 model generated by MODELLER (Fig S2) showed all residues in the allowed region as represented in Ramachandran plot (Fig. S2). Similarly, PROCHECK analysis of MUSTER model shows 97.6 % of residues (Fig. S2) in the allowed region and 2.4 % residues in the disallowed region (Laskowski et al. 1993). Furthermore, these structures were also evaluated using *Z* score calculated by ProSA-Web (Wiederstein and Sippl 2007). The *Z* score is indicative of overall model quality and measures deviation of total energy of structure (Wiederstein and Sippl 2007). The *Z* score of hECE-1 model generated by MODELLER and MUSTER was −3.25 and −0.56 as depicted in Fig. S3. The ProSA-Web result revealed that the model generated by MODELLER is in the range of native conformation with overall residue energy (Fig. S3). Structure superposition was done using PDBeFold between structures of 2PFV.pdb and N-terminal domain of TM helix model shows RMSD 1.65 Å indicating good quality of generated model (Krissinel and Henrick 2004). These results (Fig. S2 and S3) confirm that the model generated by MODELLER is better than MUSTER model and hence used to connect C-terminal domain of hECE-1.

Homodimer of hECE-1 embedded in lipid bilayer

We built a complete model of disulfide-linked (Cysteine 428) hECE-1 homodimer with transmembrane domain based on earlier experimental findings (Xu et al. 1994; Shimada et al. 1996; Valdenaire et al. 1999b; Schweizer et al. 1997; Bur et al. 2001). The mutational and immunofluorescence studies revealed that hECE-1 is localized at cell surface and highly expressed in plasma membrane (Valdenaire et al. 1999a; Schweizer et al. 1997). In our model, cysteine 428 residue is located on loop region at the surface of protein which interacts with second monomer to form disulfide bond (Fig. S4). The cysteine residues 58 and 83 of hECE-1 located on the N-terminal domain and transmembrane region, respectively, correspond to the cysteine 42 and 67 of rat ECE-1 (Shimada et al. 1996). The site-directed mutagenesis study of rat ECE-1 showed that these cysteine residues do not form either an inter-chain or an intra-chain disulfide bridge (Shimada et al. 1996). Therefore, these cysteine residues (cysteine 58 and 83) are not considered during dimer preparation (Shimada et al. 1996; Hoang et al. 1996). It has been identified that all four hECE-1 isoforms differ only in their N-terminal regions and derived from same gene through the use of alternative promoters (Schweizer et al. 1997; Valdenaire et al. 1999b). The N-terminal regions of each hECE-1 isoforms (hECE-1a–d) are differ in length with low sequence identity (Schweizer et al. 1997; Valdenaire et al. 1999b). Therefore, the first 56 residues of N-terminal domain were removed from the hECE-1 dimer. The representative model of hECE-1 devoid of N-terminal region would be applicable to all hECE-1 isoforms. The whole hECE-1 dimer modeled with transmembrane helices and C-terminal domain is depicted in Fig. S4. This final model of hECE-1 dimer embedded in POPE lipid bilayer was considered to explicit molecular dynamic simulation to check the overall stability.

MD simulation stability and secondary structure calculation of hECE-1 dimer

The molecular dynamic simulation was performed on hECE-1 dimer (devoid of N-terminal tail of 56 residues) embedded in lipid bilayer for 50 ns time scale. An initial analysis of each complex was made by the calculation of a set of standard parameters to verify simulation stability by measuring protein structure and dynamics. The root mean square deviation (RMSD) was calculated with respect to initial model of hECE-1 dimer as depicted in Fig. 2a. Initially, RMSD value of hECE-1 increased from 0.10 to 0.50 nm up to 10 ns and then retained its stability till end of simulation with small drift and plateau (Fig. 2). Analysis of individual transmembrane helices of each hECE-1 dimer shows that RMSD value lies below ~0.25 nm (Fig. 2b). These results indicate that structural arrangement of hECE-1 dimer was maintained during simulation period.

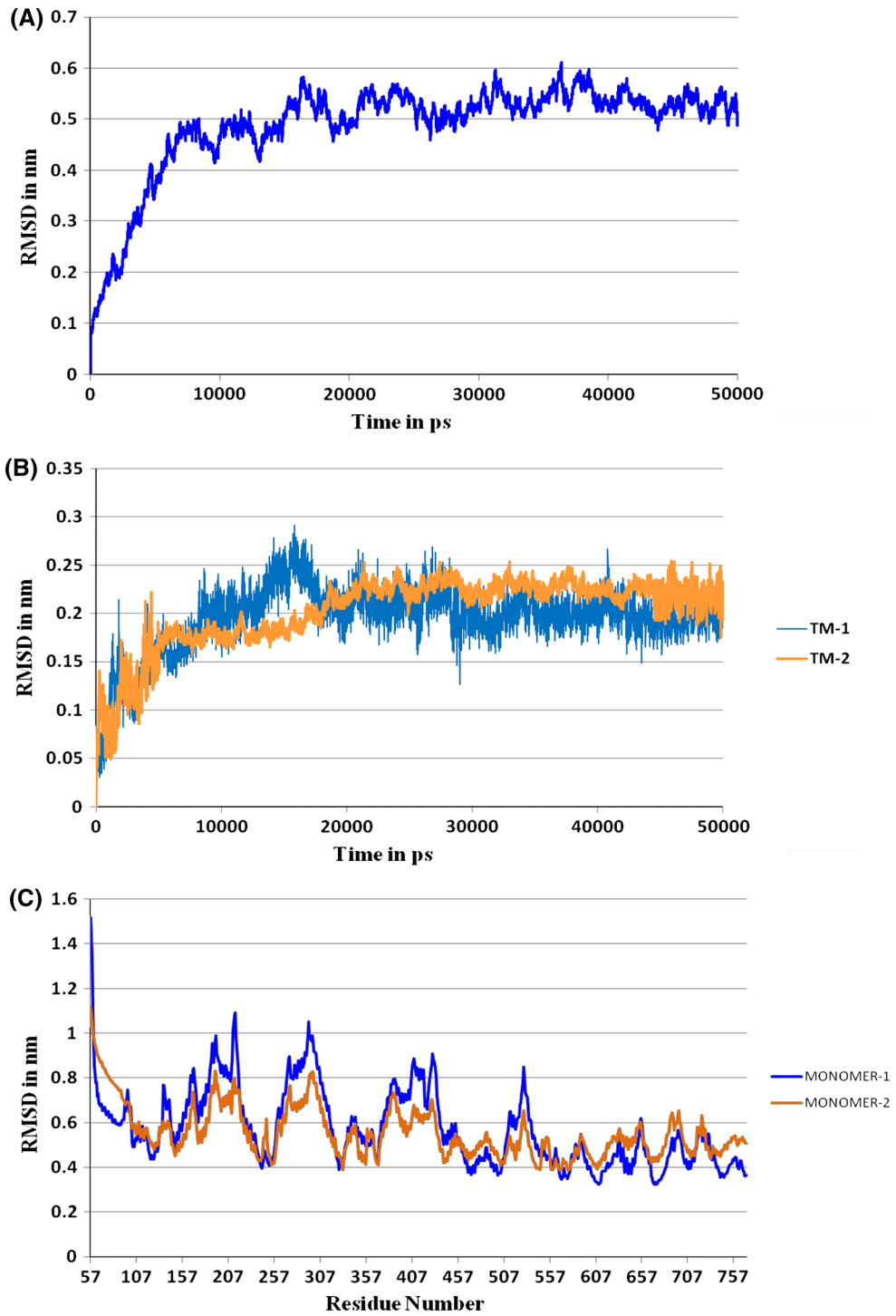

Fig. 2 **a** hECE-1-dimer backbone RMSD for 50 ns MD simulation. **b** Backbone RMSD of transmembrane helices for 50 ns MD simulation. **c** Root mean square fluctuation (RMSF) of hECE-1 residues during 50 ns MD simulation

The fluctuations of hECE-1 dimer were further investigated by calculating RMSF of Cα atoms of each residue. Figure 2c depicts RMSF values of hECE-1 monomer reflecting significant fluctuations in the loop region. The calculations of secondary structural elements were performed to correlate residue fluctuation and corresponding changes during simulation using DSSP program (Fig. 3) (Kabsch and Sander 1983). Secondary structural analysis of simulated model of hECE-1 dimer using DSSP plot (Fig. 3) shows significant differences with crystal structure (Schulz et al. 2009). The amino acid residues 69–88 comprising transmembrane helix region of hECE-1 dimer show less fluctuation by maintaining its structure throughout MD simulation (Figs. 2c, 3). After 25 ns, we have noticed that helices from residues 530–545 and 702–713 were slightly unfolded from

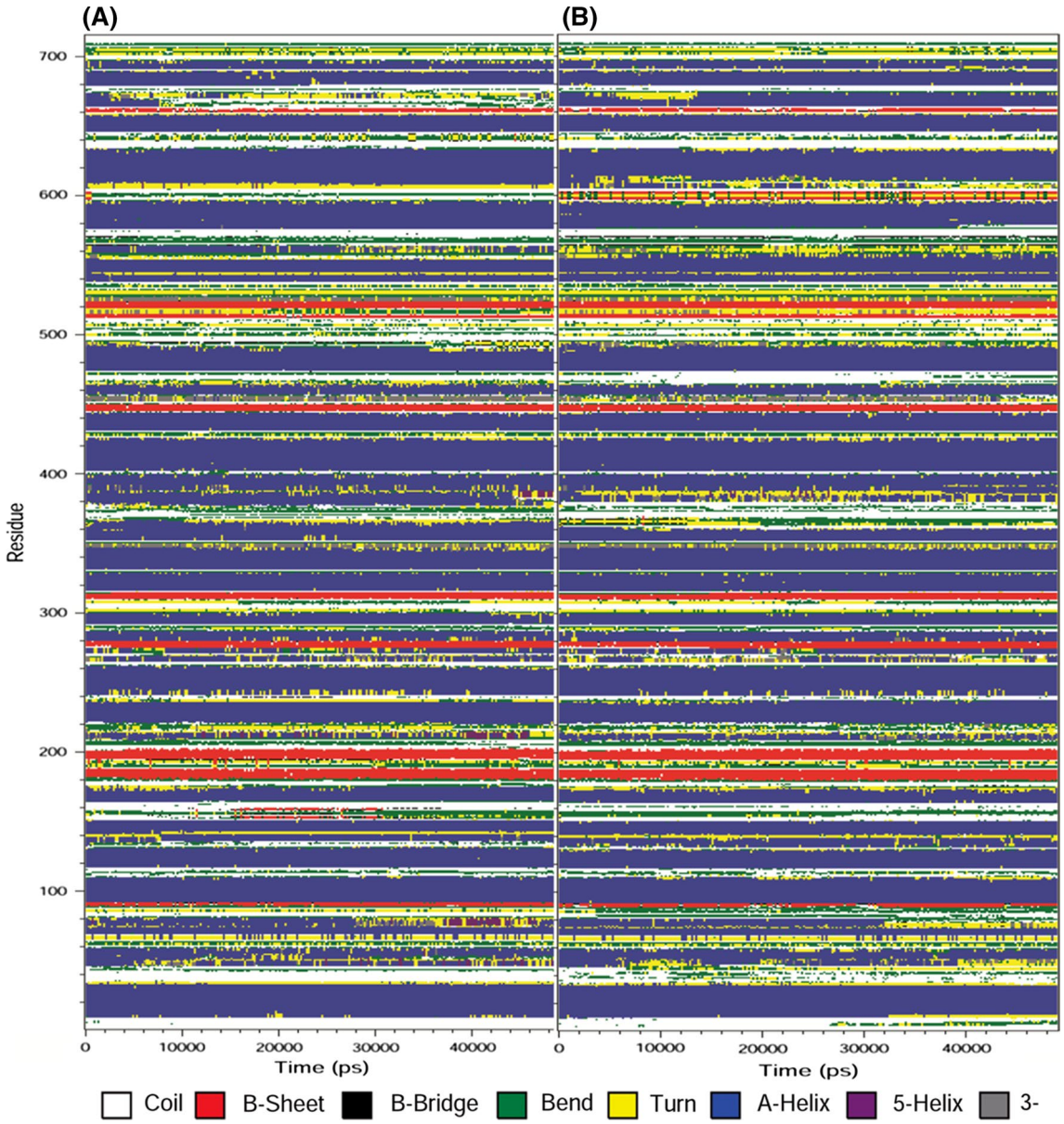

Fig. 3 The calculated secondary structure changes of hECE-1 dimer during 50 ns MD simulation by DSSP method: **a** monomer-1, **b** monomer-2

the C-terminal end. Then, another helix from residues 616–619 unfolds and refolds again to its original form (Fig. 3). Furthermore, the interdomain linker helix from 189–194 completely unfolds during the course of simulation period. In crystal structure, helical residues from 433–455 have been denoted as an interdomain linker (Schulz et al. 2009). This linker is split into two helices i.e., 439–442 and 445–456 residues during the simulation. The antiparallel β-sheet structure found at residues 238–243 and 251–256 decreases in length whereas elongation of β-sheet structure was observed at 331–335 and 366–370 residues of hECE-1. The antiparallel β-sheet structure at residue 145–147 was found at the initial stage of the simulation which was unfold and refold up to 25 ns followed by stable behavior up to the end of simulation time as per previous study (Ul-Haq et al. 2012). The secondary structural changes during MD simulation study have been found in good agreement with previous MD simulation study of extracellular domain of hECE-1 (Ul-Haq et al. 2012; Barage and Sonawane 2014; Barage et al. 2014). These DSSP results revealed that folding and unfolding as well as elongation of secondary structural elements during simulation would be essential for conformational restrains.

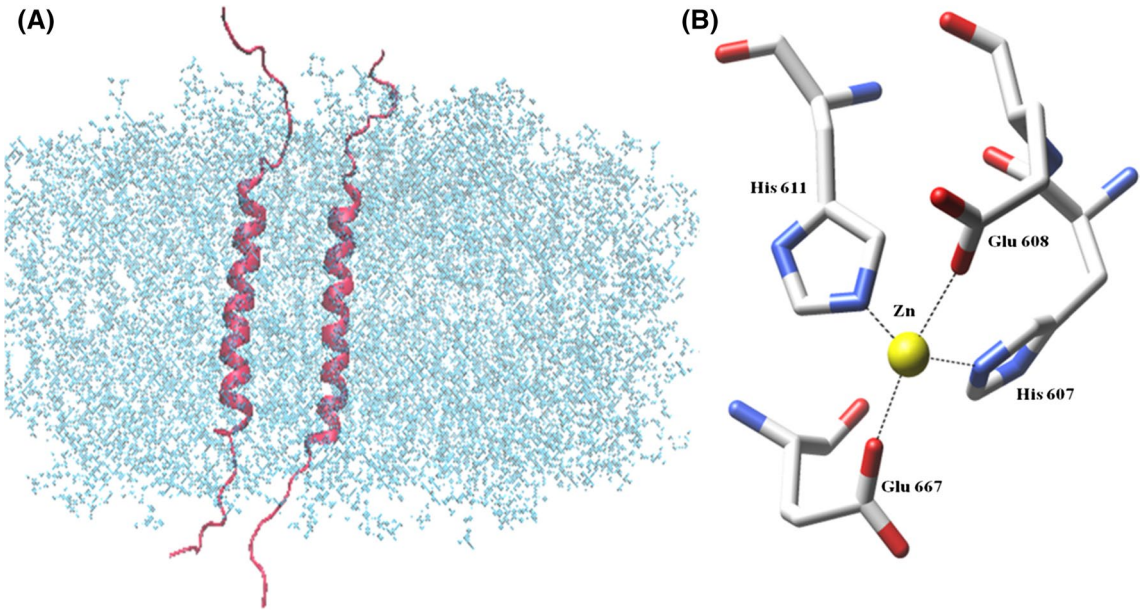

Fig. 4 **a** Conformation of TM helices after 50 ns MD simulation, **b** Zn ion (*yellow*) coordination after MD simulation with hECE-1 residues (CPK) (color figure online)

Overall structure of hECE-1 dimer after MD simulation

The MD simulation results revealed the stability of three-dimensional structure of hECE-1 dimer in lipid bilayer throughout MD simulation (Fig. S5). The residue cysteine 428 plays a crucial role in hECE-1 dimerization process as depicted in earlier experimental reports (Schulz et al. 2009; Xu et al. 1994). This cysteine 428 is located in loop regions present on the surface of the protein. These loop residues are most likely to lie within the two helices such as helix-loop-helix motif composed of two helices having one helix smaller which would increase loop flexibility for the dimerization process (Bur et al. 2001; Barage and Sonawane 2014). The helix loop transition in protein was also observed in previous computational studies (Armen et al. 2003; Shepherd and Vogel 2004; Chu and Voth 2005). The smaller helix (435–442) was transformed into loop during some part of the simulation and refolded again into helix (visual inspection) which is important to maintain hECE-1 dimer flexibility during simulation. The cysteine 428 associated loop region flexibility increases hECE-1 dimer stability as can be seen in movie (Supplementary video). The complete unfolding of N-terminal part of smaller helix and C-terminal helical part (439–442) has remained helical in nature (Fig. 3). Thus, the loop region plays an important role to maintain the dimeric structure of hECE-1. The zinc ion is observed in tetrahedral coordination geometry similar to crystal structure as depicted in Fig. 4b. In addition, TM helices are located entirely within the hydrophobic core of the lipid bilayer. The TM helices show α-helical conformation with its helical axis perpendicular to the bilayer plane throughout simulation time (Fig. 4a).

The analysis of extracellular C-terminal domain to elucidate dynamic motion of central cavity, and pockets (S1 and S2) associated with it. The accurate computation of solvent accessible surface (SA, Richards' surface) and molecular surface (MS, Connolly's surface) has been done by an alpha shape method (Dundas et al. 2006). These results show that enzyme has total central cavity volume around 13,200 $Å^3$ and 4,798 $Å^2$ area for substrate molecule as depicted in Fig. 5a. However, no significant differences were observed in S1 and S2 pockets size. The variation in the volume and area of the central cavity of hECE-1 dimer is due to certain conformational changes observed during simulation. We have noted some conformational changes at interdomain linker helices, such as complete unfolding of interdomain helix (189–194) followed by conformational changes at loop associated helices as discussed above. The slight unfolding of N-terminal region of helix at residues 530–545 and 702–713 was also observed during simulation. These conformational rearrangements between interdomain linker helices as well as helices close to the inner surface of protein may contribute to conformational restrains on enzyme resulted in the increase of total central cavity as compared to previous MD simulation study of extracellular domain of hECE-1 monomer (Barage and Sonawane 2014). These results are in close agreement with previous experimental report which showed

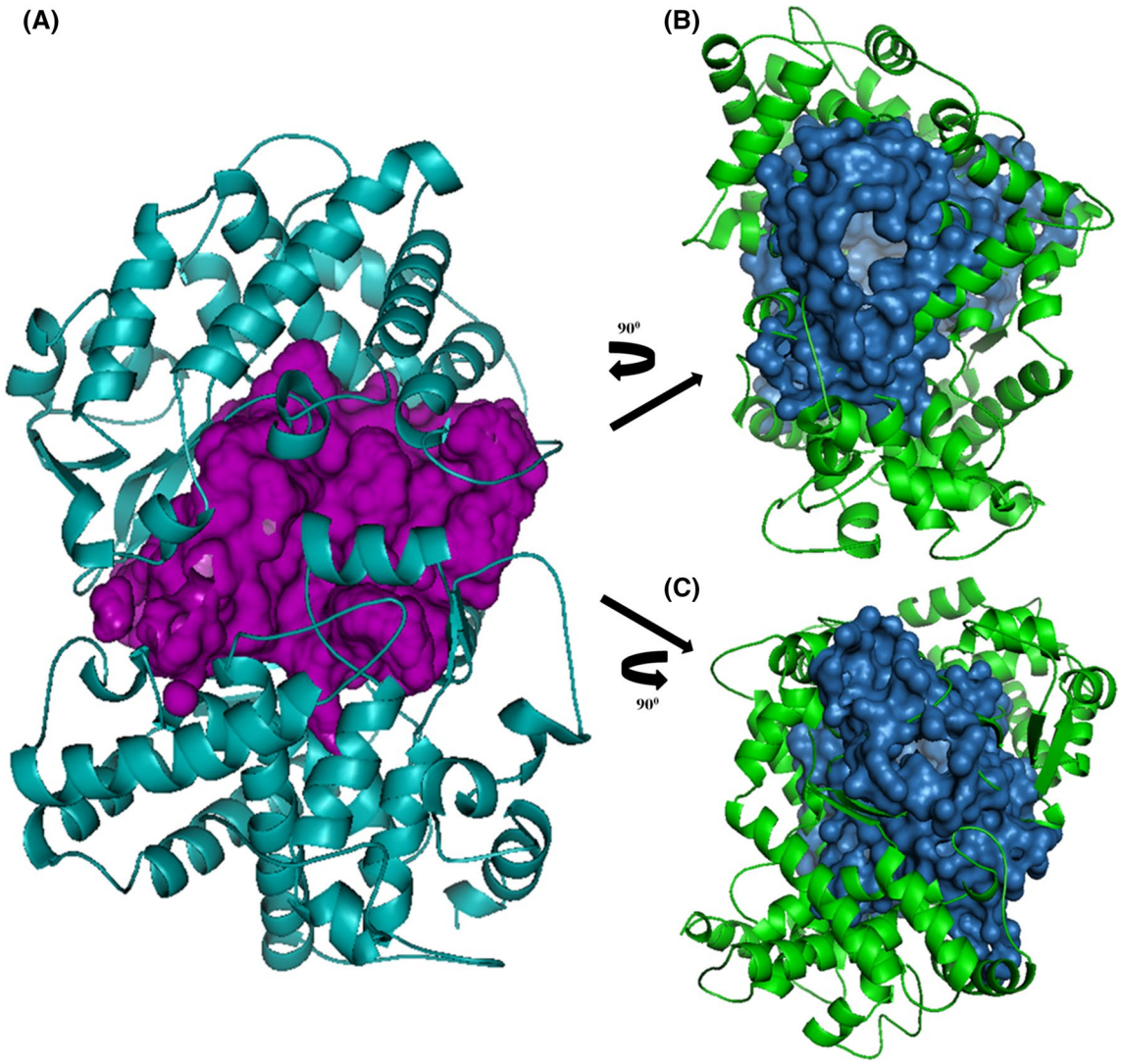

Fig. 5 **a** Surface region showing central spherical cavity (*magenta color*) and protein shown in forest *green color*. **b** Spherical cavity opening after 90° clockwise rotation of hECE-1 monomer with respect to cysteine 428. **c** Spherical cavity opening after 90° anticlockwise rotation of hECE-1 monomer with respect to cysteine 428 (color figure online)

that monomeric hECE-1 has a lower affinity for substrates and inhibitors as compared with dimeric hECE-1 (Shimada et al. 1996).

The secondary structural elements associated with three active site motifs HExxH, ExxxD and NAY/FY involved in substrate interaction remain stable throughout simulation time (Bur et al. 2001; Schulz et al. 2009; Sansom et al. 1998), while R145 located on antiparallel β-sheet at residue 145–147 shows conformational changes up to 25 ns followed by stable behavior in the rest of simulation as per the previous computational study (Ul-Haq et al. 2012). The conformational stability of secondary structure element associated with the active site motif suggests that these residues work as central determinant for hECE-1 activity.

Analysis of possible substrate entry/exit sites

CASTp server (Dundas et al. 2006) has been used to identify possible substrate/product entry/exit sites of hECE-1 dimer. We have observed two significant openings on the surface of protein accessible to the active site of hECE-1 (Fig. 5b, c). The first pocket mouth was observed in between antiparallel β-sheet (238–243 and 251–256) structure located at the opposite site of disulfide bond of homodimer (Fig. 5b). These antiparallel β-sheet structures are separated by loop region at residues 244–250. The conformational rearrangement of these β-sheet structures increases loop flexibility during simulation period. The degree of fluctuation exhibited by this region controls the opening of pocket mouth. The second possible entry/exit

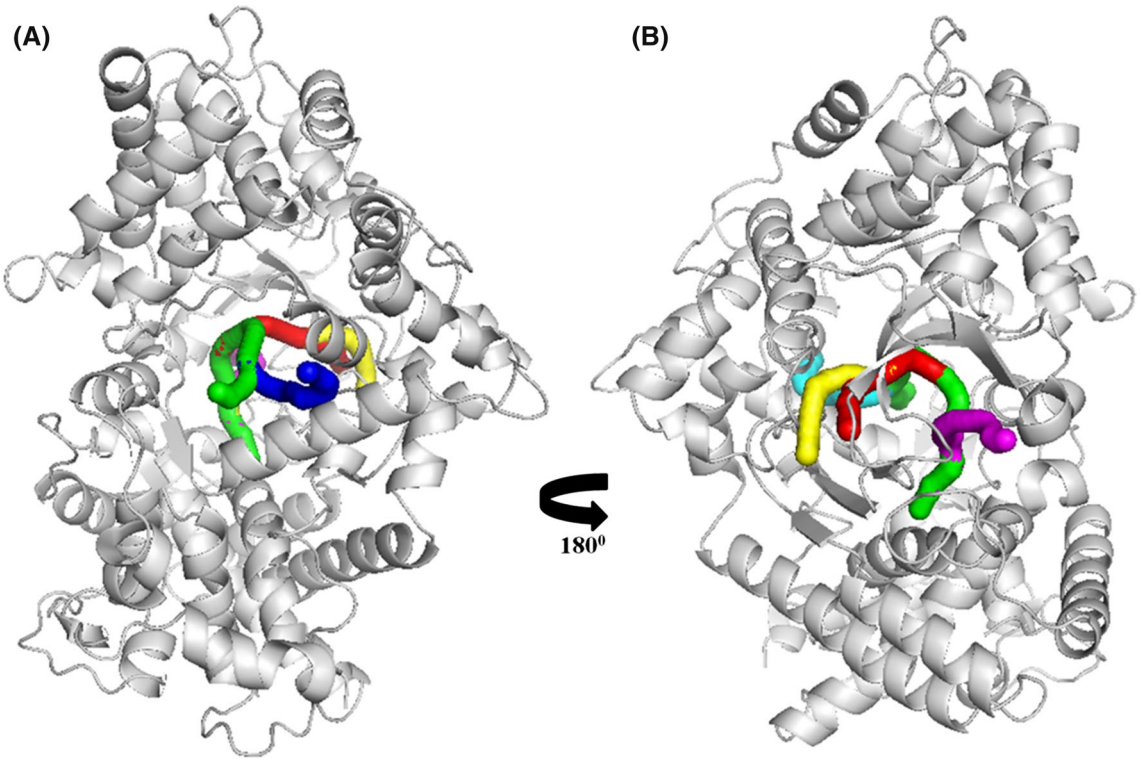

Fig. 6 Showing accessible entry/exit path for substrate/product towards active site characterized with CAVER using atomic coordinates of C-terminal domain of simulated hECE-1 dimer. **a** Two tunnels below cysteine 428. **b** Three tunnels after 180° rotation of hECE-1 monomer with respect to cysteine 428

site might be situated below the loop region which involved in the dimerization process (Fig. 5c).

CAVER analysis was also made to predict the possible tunnels through which active site of enzyme can be accessed. In this respect, we have considered the key residues involved in catalysis of substrate during prediction of possible tunnels for entry/exit sites of the substrate/product towards an active site as per previous experimental study using CAVER (Schulz et al. 2009; Johnson et al. 2002). In our analysis, five possible tunnels were identified among the top ranked clusters (Fig. 6). The obtained results are in good agreement with our CASTp analysis (Fig. 5). Based on these results, we found that hECE-1 dimer could have two possible entry/exit sites to access or leave the substrate/product from the catalytic site of enzyme. We thought that these conformational changes are relevant for substrate entry to access catalytic site as explained in previous report of LinB (Negri et al. 2007). Thus, MD simulation of hECE-1 dimer with lipid bilayer helped to shed some light on the conformation and dynamic behavior.

Molecular docking and MD simulation of hECE-1 and $A\beta_{1-42}$ complex

Alzheimer's disease (AD) is a neurodegenerative disorder characterized by abnormal accumulation of the Aβ peptide in brain (Hardy and Selkoe 2002; Hardy 2009; Karran et al. 2011). Experimentally, it has been reported that hECE-1 is involved in the degradation of Aβ peptide (Eckman et al. 2001; Eckman and Eckman 2005). Therefore, the degradation ability of hECE-1 could be an effective alternative to reduce Aβ load in AD brain (Evin and Weidemann 2002; Vardy et al. 2005; Nalivaeva et al. 2012). The previous experimental studies revealed that Aβ monomer favors α-helix structure in a membrane or membrane-mimicking environment (Coles et al. 1998; Xu et al. 2005). Subsequently, within plaque Aβ peptides in β-sheet conformation assemble and polymerize into structurally distinct forms, including fibrillar, protofibers and polymorphic oligomers (Xu et al. 2005). In this regard, we have selected full length Aβ peptide structure having α-helix conformation. Moreover, obtaining model with larger substrate such as Aβ-peptide is quite difficult due to extensive conformational space of Aβ peptide and catalytic groove of hECE-1 as explained in earlier studies (Barage and Sonawane 2014; Barage et al. 2014). The molecular docking has been performed between simulated structure of hECE-1 dimer and three different conformations of Aβ peptide extracted from 1AML.pdb, 1BA4.pdb and 1IYT.pdb, respectively. We have analyzed all docked conformations to understand binding mode of Aβ peptide in catalytic groove of hECE-1

Table 1 Results of docking calculation of three Aβ peptide structures with hECE-1

Sr. No	Docked complex	Mean binding energy (kcal/mol)
1.	hECE-1 and 1AML.pdb	+11,573.02
2.	hECE-1 and 1BA4.pdb	+2.37e+06
3.	hECE-1 and 1IYT.pdb	−1.77e+07

along with binding energy (Table 1). Among them, complex of hECE-1 with 1IYT.pdb shows required interactions and lowest binding energy with hECE-1. However, in other complexes of hECE-1 along with 1AML.pdb and 1BA4.pdb, Aβ peptide could not completely be entrapped in substrate-binding channel of hECE-1 and showed the highest binding energy (Table 1). The analysis of bound conformation of $A\beta_{1-42}$ peptide shows that side chains of $A\beta_{1-42}$ peptide residues properly accommodate in the active site of hECE-1 dimer (Fig. 7). The N-terminal and C-terminal regions of $A\beta_{1-42}$ peptide have been observed in between two surface openings of hECE-1as predicted by CASTp analysis (Fig. 5b).

The molecular dynamics simulation has been performed over the docked complex of hECE-1 dimer along with two molecules of $A\beta_{1-42}$ peptide. We have analyzed complex of hECE-1 dimer and $A\beta_{1-42}$ after MD simulation. The overall bound conformation of $A\beta_{1-42}$ peptide selectively entraps in hECE-1 substrate binding channel (Schulz et al. 2009; Barage et al. 2014). The hydrogen bonding network between $A\beta_{1-42}$ peptide and hECE-1 residues has been observed in both monomers (Fig. 8; Tables 2, 3). Interestingly, total 11 residues of hECE-1 such as His 143, Arg 145, Arg 324, Arg 325, Glu 327, Val 565, Asn 566, Thr 572, Thr 729, Asp 730 and His 732 interact with $A\beta_{1-42}$ peptide residues in both monomers (Fig. 8; Tables 2, 3) similar to previous MD simulation study (Barage et al. 2014), while additional hydrogen bonding interactions have been observed between Ser 144, Arg 718, Glu 440 residues of monomer-1 (Fig. 8a; Table 2) and Ser 437, Asn 441, Ser 722 of monomer-2 (Fig. 8b; Table 3) with $A\beta_{1-42}$ peptide. These results revealed that $A\beta_{1-42}$ peptide is properly accommodated in the active site of hECE-1 and stabilized by hydrogen bonding network with hECE-1 residues. The observed positions and orientation of $A\beta_{1-42}$ peptide residues in catalytic groove of hECE-1 facilitate cleavage of $A\beta_{1-42}$ peptide and reduce Aβ load in AD brain.

Analysis of binding free energy of hECE-1 and $A\beta_{1-42}$ complex

The molecular docking followed by MD simulation presents the most time demanding step for binding free energy evaluation as reported earlier (Bonnet and Bryce 2004; Donini and Kollman 2000). The ΔG values averaged over

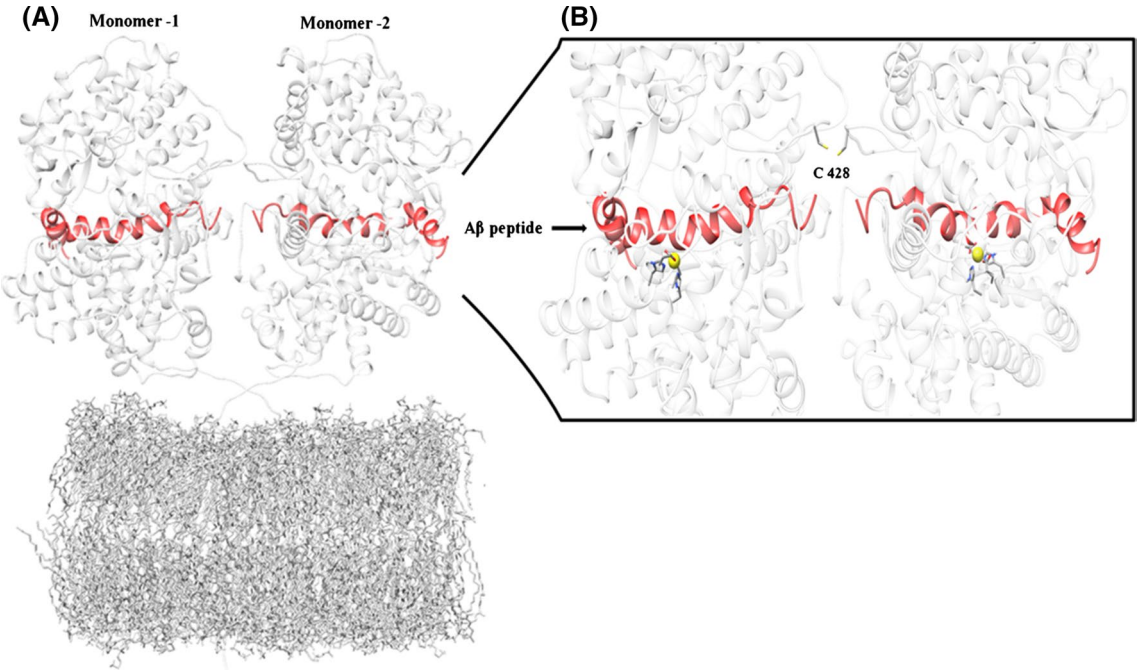

Fig. 7 The bound conformation of $A\beta_{1-42}$ to hECE-1 dimer. **a** hECE-1 dimer embedded in lipid bilayer, $A\beta_{1-42}$ (*red*), **b** a view of the active site of hECE-1 dimer, Zn ion (*yellow*), C428 (*ball* and *stick*) (color figure online)

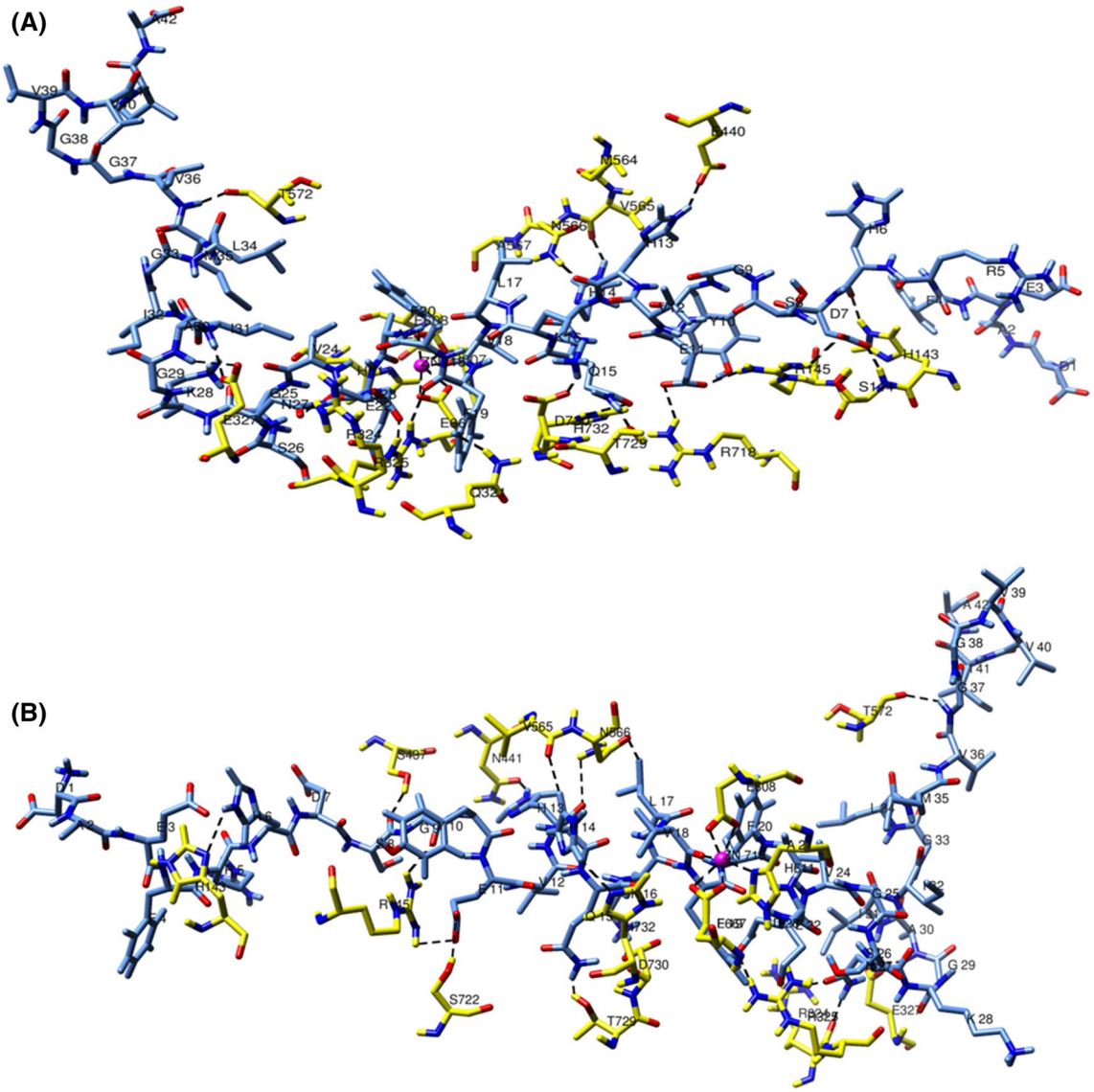

Fig. 8 The intramolecular hydrogen bonding interaction between hECE-1 residue (*yellow*) and $A\beta_{1-42}$ peptide (*cornflower blue*), Zn ion colored in *magenta*. **a** Monomer-1, **b** Monomer-2 (color figure online)

sets of snapshot generated through MD simulation which naturally takes into account the fluctuation of protein and ligand complex conformation and ensures a proper adjustment of ligand in binding site are described in previous publication (Bonnet and Bryce 2004; Vorontsov and Miyashita 2011). Therefore, to validate binding modes of hECE-1 with $A\beta_{1-42}$ peptide, the electrostatic, van der Waals and solvation energy of interacting residues have been calculated using MM/PBSA method (Hou et al. 2011; Spiliotopoulos et al. 2012). The MM/PBSA calculation of hECE-1 and $A\beta_{1-42}$ peptide complex produces favorable ΔG values in the range of −300 to −500 kcal/mol can be clearly seen from Fig. 9. The binding energy shows slight variation in each snapshot because conformational space is not sampled enough to obtain converged results. Hou coworkers reported that extending simulation time does not always improve the correlations between the predicted binding free energies and the experimental values (Hou et al. 2011; Genheden and Ryde 2010). For some system, binding free energy of short MD simulation is even slightly better than that based on longer MD simulation. The contribution of hECE-1 residues in both the monomers around the active site can be clearly seen from Fig. 10. The electrostatic interactions play a major role in hydrogen bond formation. Especially, the electrostatic energies (ΔE_{ele}) of hECE-1 residues such as His 143, Arg 145, Arg 324, Arg 325, Glu 327, Val 565, Asn 566, Thr 572, Thr 729, Asp 730 and His 732 contribute prominently which might be

Table 2 Hydrogen bonding interactions between hECE-1 and $A\beta_{1-42}$ peptide residues in monomer-1

Residue name	Distance (Å)
His 143HE2……O His 6	1.897
Ser 144 H……OD1 Asp 7	1.893
Arg 145 1HH2……OD2 Asp 7	2.722
Arg 145 1HH1……OE2 Glu11	2.998
Arg 718 1HH1……OE1Glu 11	2.638
Thr 729 OG1……2HE2 Gln 15	1.735
Asp 730 OD2……HZ2 Lys 16	2.092
Arg 325 HE……OD1 Asp 23	2.091
Arg 325 1HH2……O Phe 19	2.447
Arg 324 2HH2……OD1 Asn 27	2.228
Glu 327 OE2……H Ile 31	2.157
Glu 327 OE1……H Ala 30	2.412
Val 565 O……HE2 His 14	1.855
Asn 566 2HD2……O His 13	1.910
Glu 440 OE1……HE2 His 13	1.795
Thr 572 O…… H Val 36	2.739
His 732 HD1……OE1 Gln 15	2.531

Table 3 Hydrogen bonding interactions between hECE-1 and $A\beta_{1-42}$ peptide residues in monomer-2

Residue name	Distance (Å)
His 143 ND1……HE2 His 6	2.810
Arg 145 1HH2……O Gly 9	2.786
Arg 145 1HH1……OE2 Glu 11	2.317
Arg 325 1HH1……OD1 Asn 27	2.467
Arg 325 2HH2……OD2 ASP 23	1.834
Arg 324 O……2HD2 Asn 27	1.681
Glu 327 OE2……H Ala 30	2.369
Glu 327 OE1……H Ile 31	2.073
Val 565 O……HD2 His 14	2.398
Asn 566 1HD2……O His 13	2.933
Ser 437 HG……O Ser 8	1.799
Asn 441 OD1……HE2 His 13	1.867
Thr 572 O……H Gly 37	2.291
Ser 722 HG……OE1 Glu 11	2.652
Thr 729 HG1……2HE2 Gln 15	1.995
Asp 730 OD1…….HZ3 Lys 16	2.388
His 732 NE2……HE1 His 14	2.712

responsible for the formation of several hydrogen bonds with $A\beta_{1-42}$ peptide as shown in the Fig. 10 (Schulz et al. 2009; Sansom et al. 1998; Barage et al. 2014). In addition to this, favorable van der Waals contributions are also associated with these residues. These results suggest that hECE-1 residues interact with $A\beta_{1-42}$ peptide. However, other amino acids such as Ser 144, Arg 718, Glu 440 of monomer-1 and Ser 437, Asn 441, Ser 722 of monomer-2 show negligible energetic contributions. These results revealed that hECE-1 has charged binding pocket consisting of three Arg, one Glu and one Asp. These residues form strong ionic interactions with oppositely charged amino acids of substrate. Therefore, strong electrostatic potential is present at binding interface of hECE-1 active site.

The bound conformation of hECE-1 and $A\beta_{1-42}$ peptide revealed that the side chains of $A\beta_{1-42}$ peptide residues properly accommodate in the active site of the enzyme through hydrogen bonding and hydrophobic interactions. The N-terminal and C-terminal regions of $A\beta_{1-42}$ peptide have been observed in the two surface openings of hECE-1 as predicted by CASTp and CAVER analysis (Figs. 7, 8). These results revealed that, predicted entry/exit sites are useful to facilitate entry/exit of substrate/product towards the active site of the enzyme in each hECE-1 monomer. In view of all of the above results, the conformational changes occurred in interior of the enzyme and surface of hECE-1 dimer during simulation could be helpful to expand total central cavity associated with the active site of hECE-1. Taken together, these findings suggest that hECE-1 prefers membrane-bound dimeric structure for effective conversion of substrate. This study offers valuable information about $A\beta_{1-42}$ peptide interaction with hECE-1 time and extends our views to consider hECE-1 as a therapeutic option in AD.

Conclusion

The membrane-bound dimeric structure of hECE-1 was found stable throughout MD simulation. The C428 located in the loop region lies within the helix-loop-helix motif, which might enhance flexibility and stability of dimeric hECE-1 embedded in lipid bilayer. Simulation of hECE-1 dimer revealed distinct conformational changes in secondary structural elements at the surrounding of active site residues and some surface regions of protein. Three active site motifs retained their conformations during simulation period which might have role in the catalysis of substrate. The residue R145 plays an important role in substrate binding through conformational transition from loop to antiparallel β-sheet. The conformational changes occur near the active site surrounded by helices (474–489 and 646–657) along with interdomain linkers. This could be responsible for expanding the total central cavity of hECE-1. The two possible entry/exit sites were observed in hECE-1 dimer through which substrate/product can access or leave the active site of the enzyme. The conformational rearrangements of antiparallel β-sheets present on the surface region might assist the movement of loop region and entrance/exit of substrate/product.

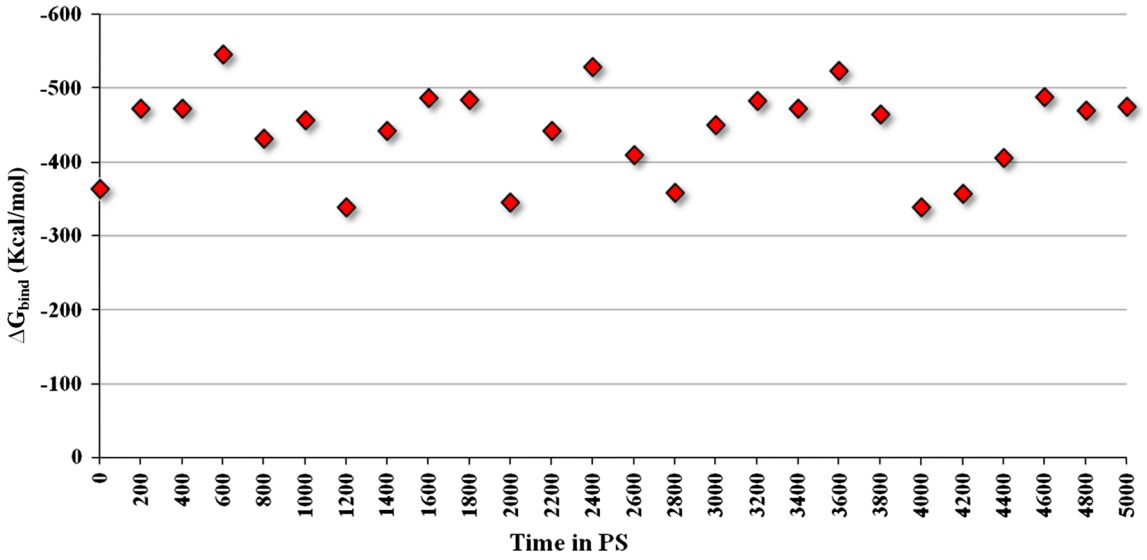

Fig. 9 MM/PBSA estimated binding free energy of hECE-1 and $A\beta_{1-42}$ complex throughout simulation time

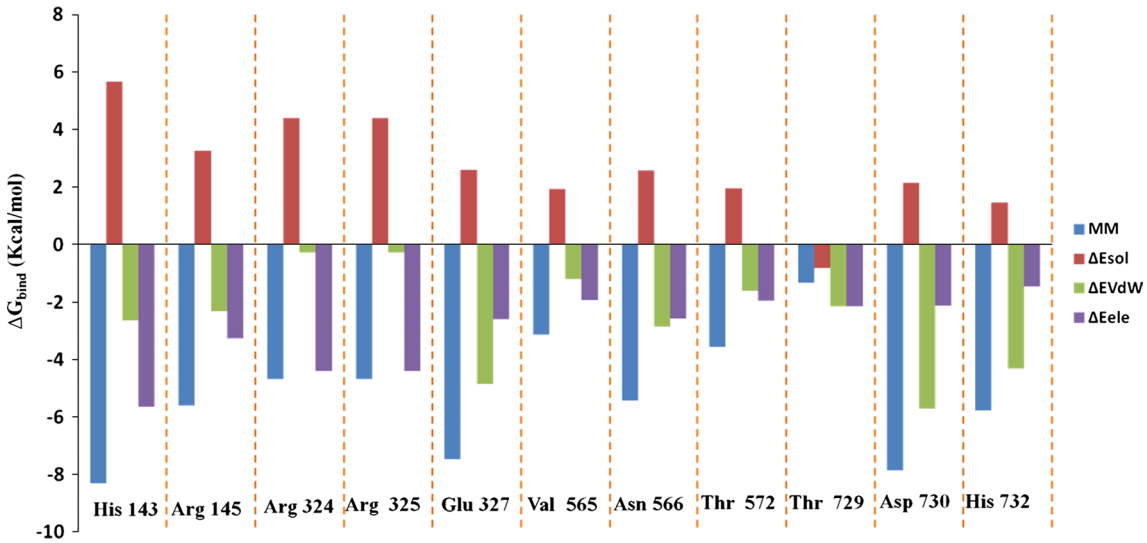

Fig. 10 Decomposition of the binding free energy as per basis of hECE-1 residues

The binding free energy calculation study of MD simulated hECE-1 and $A\beta_{1-42}$ peptide complex revealed higher binding affinity of $A\beta_{1-42}$ peptide towards hECE-1 residues. The residue decomposition analysis illustrates that His 143, Arg 145, Arg 324, Arg 325, Glu 327, Val 565, Asn 566, Thr 572, Thr 729, Asp 730 and His 732 are the key residues of hECE-1 which are involved in binding with $A\beta_{1-42}$ peptide. This simulation study of hECE-1 with $A\beta_{1-42}$ peptide provides valuable information about the bound conformation of $A\beta_{1-42}$ peptide to catalytic groove of hECE-1. Thus, the present study sheds light on the structural aspects and dynamics of hECE-1 dimer which might be helpful to design varied approaches to target hECE-1 in the treatment of Alzheimer's diseases.

Acknowledgments KDS gratefully acknowledges the University Grand Commission, New Delhi for financial support under the UGC major research project. The authors are very much thankful to Computer Centre, Shivaji University, Kolhapur for providing computational facility.

Conflict of interest All authors have no conflict of interest.

References

Ahn K, Beningo K, Olds G, Hupe D (1992) The endothelin-converting enzyme from human umbilical vein is a membrane-bound metalloprotease similar to that from bovine aortic endothelial cells. Proc Natl Acad Sci USA 89:8606–8610

Altschul SF, Madden TL, Schäffer AA (1997) Gapped BLAST and PSI-BLAST: a new generation of protein database search programs. Nucleic Acids Res 25:3389–3402

Armen R, Alons DOV, Daggett V (2003) The role of α-, 310-, and π-helix in helix–coil transitions. Protein Sci 12:1145–1157

Barage SH, Sonawane KD (2014) Exploring mode of phosphoramidon and Aβ peptide binding to hECE-1 by molecular dynamics and docking studies. Protein Pept Lett 21:140–152

Barage SH, Jalkute CB, Dhanavade MJ, Sonawane KD (2014) Simulated interactions between endothelin converting enzyme and Aβ peptide: insights into subsite recognition and cleavage mechanism. Int J Pept Res Ther 20:409–420

Bonnet P, Bryce RA (2004) Molecular dynamics and free energy analysis of neuraminidase–ligand interactions. Prot Sci 13:946–957

Bur D, Dale GE, Oefner C (2001) A three-dimensional model of endothelin-converting enzyme (ECE) based on the X-ray structure of neutral endopeptidase 24.11 (NEP). Protein Eng 14:337–341

Cavasotto CN, Phatak SS (2009) Homology modeling in drug discovery: current trends and applications. Drug Discov Today 14:676–683

Chovancova E, Pavelka A, Benes P, Strnad O, Brezovsky J, Kozlikova B, Gora A, Sustr V, Klvana M, Medek P, Biedermannova L, Sochor J, Damborsky J (2012) CAVER 3.0: a tool for the analysis of transport pathways in dynamic protein structures. PLoS Comput Biol 8:e1002708

Chu JW, Voth GA (2005) Allostery of actin filaments: molecular dynamics simulations and coarse-grained analysis. PNAS 102:13111–13116

Coles M, Bicknell W, Watson AA, Fairlie DP, Craik DJ (1998) Solution structure of amyloid beta-peptide (1–40) in a water-micelle environment. Is the membrane-spanning domain where we think it is? Biochemistry 37:11064–11077

Crescenzi O, Tomaselli S, Guerrini R, Salvadori S, D'Ursi AM, Temussi PA, Picone D (2002) Solution structure of the Alzheimer amyloid beta-peptide (1–42) in an apolar microenvironment. Similarity with a virus fusion domain. Eur J Biochem 269:5642–5648

Dhanavade MJ, Sonawane KD (2014) Insights into the molecular interactions between aminopeptidase and amyloid beta peptide using molecular modeling techniques. Amino Acids. doi:10.1007/s00726-014-1740-0

Dhanavade MJ, Jalkute CB, Barage SH, Sonawane KD (2013) Homology modeling, molecular docking and MD simulation studies to investigate role of cysteine protease from *Xanthomonas campestris* in degradation of Aβ-peptide. Comput Biol Med 43:2063–2070

Domene C, Furini S (2012) Molecular dynamics simulations of the TrkH membrane protein. Biochemistry 51:1559–1565

Donini OA, Kollman PA (2000) Calculation and prediction of binding free energies for the matrix metalloproteinases. J Med Chem 43:4180–4188

Dundas J, Ouyang Z, Tseng J, Binkowski A, Turpaz Y, Liang J (2006) CASTp: computed atlas of surface topography of proteins with structural and topographical mapping of functionally annotated residues. Nucleic Acids Res 34:116–118

Eckman EA, Eckman CB (2005) Aβ-degrading enzymes: modulators of Alzheimer's disease pathogenesis and targets for therapeutic intervention. Biochem Soc Trans 33:1101–1105

Eckman EA, Reed DK, Eckman CB (2001) Degradation of the Alzheimer's amyloid-β peptide by endothelin-converting enzyme. J Biol Chem 276:24540–24548

Essmann U, Perera L, Berkowitz ML, Darden T, Lee H, Pedersen LG (1995) A smooth particle mesh Ewald method. J Chem Phys 103:8577–8593

Evin G, Weidemann A (2002) Biogenesis and metabolism of Alzheimer's disease Abeta amyloid peptides. Peptides 23:1285–1297

Faraldo-Gomez JD, Smith GR, Sansom MS (2002) Setting up and optimization of membrane protein simulations. Eur Biophys J 31:217–227

Garnier J, Gibrat JF, Robson B (1996) GOR method for predicting protein secondary structure from amino acid sequence. Methods Enzymol 266:540–553

Genheden S, Ryde U (2010) How to obtain statistically converged MM/GBSA results. J Comput Chem 31:837–846

Geourjon C, Deleage G (1995) SOPMA: significant improvements in protein secondary structure prediction by consensus prediction from multiple alignments. Comput Appl Biosci 11:681–684

Grossman M, Born B, Heyden M, Tworowski D, Fields GB, Sagi I, Havenith M (2011) Correlated structural kinetics and retarded solvent dynamics at the metalloprotease active site. Nat Struct Mol Biol 18:1102–1108

Hall TA (1999) BioEdit: a user-friendly biological sequence alignment editor and analysis program for Windows 95/98/NT. Nucleic Acids Symp Sers 41:95–98

Hans-Dieter O, Richter CM, Funke-Kaiser H, Kröger B, Schmidt M, Menzel S, Bohnemeier H, Paul M (1997) Evidence of alternative promoters directing isoform-specific expression of human endothelin-converting enzyme-1 mRNA in cultured endothelial cells. J Mol Med 75:512–521

Hardy J (2009) The amyloid hypothesis for Alzheimer's disease:a critical reappraisal. J Neurochem 110:1129–1134

Hardy J, Selkoe DJ (2002) The amyloid hypothesis of Alzheimer's disease: progress and problems on the road to therapeutics. Science 297:353–356

Henin J, Pohorille A, Chipot C (2005) Insights into the recognition and association of transmembrane α-helices. The free energy of α-helix dimerization in glycophorin A. J Am Chem Soc 127:8478–8484

Hess B (2008) P-LINCS: a parallel linear constraint solver for molecular simulations. J Chem Theor Comput 4:116–122

Hillisch A, Pineda LF, Hilgenfeld R (2004) Utility of homology models in the drug discovery process. Drug Discov Today 9:659–669

Hoang VM, Sansom CE, Turner AJ (1996) Mutagenesis and modelling of endothelin converting enzyme. Biochem Soc Trans 24:471S

Hou T, Wang J, Li Y, Wang W (2011) Assessing the performance of the MM/PBSA and MM/GBSA methods. 1. The accuracy of binding free energy calculations based on molecular dynamics simulations. J Chem Inf Model 51:69–82

Hu X, Shelver WH (2003) Docking studies of matrix metalloproteinase inhibitors: zinc parameter optimization to improve the binding free energy prediction. J Mol Graph Model 22:15–126

Humphrey W, Dalke A, Schulten K (1996) VMD: visual molecular dynamics. J Mol Graph 14:33–38

Inoue A, Yanagisawa M, Kimura S, Kasuya Y, Miyauchi T, Goto K, Masaki T (1989) The human endothelin family: three structurally and pharmacologically distinct isopeptides predicted by three separate genes. Proc Natl Acad Sci USA 86:2863–2867

Irwin JJ, Raushel FM, Shoichet BK (2005) Virtual screening against metalloenzymes for inhibitors and substrates. Biochemistry 44:12316–12328

Jalkute CB, Barage SH, Dhanavade MJ, Sonawane KD (2013) Molecular dynamics simulation and molecular docking studies of

angiotensin converting enzyme with inhibitor lisinopril and amyloid beta peptide. Protein J 3:356–364
Johnson GD, Stevenson T, Ahn K (1999) Hydrolysis of peptide hormones by endothelin-converting enzyme-1. J Biol Chem 274:4053–4058
Johnson GD, Swenson HR, Ramage R, Ahn K (2002) Mapping the active site of endothelin converting enzyme-1 through subsite specificity and mutagenesis studies: a comparison with neprilysin. Arch Biochem Biophys 398:240–248
Kabsch W, Sander C (1983) Dictionary of protein secondary structure: pattern recognition of hydrogen-bonded and geometrical features. Biopolymers 22:2577–2637
Kandt C, Ash WL, Tieleman DP (2007) Setting up and running molecular dynamics simulations of membrane proteins. Methods 41:475–488
Karran E, Mercken M, De Strooper B (2011) The amyloid cascade hypothesis for Alzheimer's disease: an appraisal for the development of therapeutics. Nat Rev Drug Discov 10:698–712
Kedzierski RM, Yanagisawa M (2001) Endothelin system: the double-edged sword in health and disease. Annu Rev Pharmacol Toxicol 41:851–876
Khemili S, Kwasigroch JM, Hamadouche T, Gilis D (2012) Modelling and bioinformatics analysis of the dimeric structure of house dust mite allergens from families 5 and 21: Der f 5 could dimerize as Der p 5. J Biomol Struct Dyn 29:663–675
Kirkby NS, Hadoke PWF, Bagnall AJ, Webb DJ (2008) The endothelin system as a therapeutic target in cardiovascular disease: great expectations or bleak house. Br J Pharmacol 153:1105–1119
Krissinel E, Henrick K (2004) Secondary-structure matching (SSM): a new tool for fast protein structure alignment in three dimensions. Acta Crystallogr D Biol Crystallogr 60:2256–2268
Krogh A, Larsson B, Von Heijne G, Sonnhammer EL (2001) Predicting transmembrane protein topology with a hidden markov model: application to complete genomes. J Mol Biol 305:567–580
Krum H, Viskoper RJ, Lacourciere Y, Budde M, Charlon V (1998) The effect of an endothelin-receptor antagonist, bosentan, on blood pressure in patients with essential hypertension. N Engl J Med 338:784–790
Lambert LA, Whyteside AR, Turner AJ, Usmani BA (2008) Isoforms of endothelin converting enzyme-1 (ECE-1) have opposing effects on prostate cancer cell invasion. Br J Cancer 99:1114–1120
Laskowski RA, MacArthur MW, Moss DS, Thornton JM (1993) PROCHECK—a program to check the stereochemical quality of protein structures. J Appl Cryst 26:283–291
Miners JS, Barua N, Kehoe PG, Gill S, Love S (2011) Aβ-degrading enzymes: potential for treatment of Alzheimer disease. J Neuropathol Exp Neurol 70:944–959
Moore BA, Robinson HH, Xu Z (2007) The crystal structure of mouse Exo70 reveals unique features of the mammalian exocyst. J Mol Biol 371:410–421
Morris GM, Huey R, Lindstrom W, Sanner MF, Belew RK, Goodsell DS, Olson AJ (2009) AutoDock4 and AutoDockTools4: automated docking with selective receptor flexibility. J Comput Chem 30:2785–2791
Nalivaeva N, Beckett C, Belyaev ND, Turner AJ (2012) Are amyloid degrading enzymes viable therapeutic targets in Alzheimer's disease? J Neurochem 120:167–185
Negri A, Marco E, Damborsky J, Gago F (2007) Stepwise dissection and visualization of the catalytic mechanism of haloalkane dehalogenase LinB using molecular dynamics simulations and computer graphics. J Mol Graph Model 26:643–651
Ohnaka K, Takayanagi R, Nishikawa M, Haji M, Nawata H (1993) Purification and characterization of a phosphoramidon-sensitive endothelin-converting enzyme in porcine aortic endothelium. J Biol Chem 268:26759–26766
Papakyriakou A, Spyroulias GA, Sturrock ED, Zoupa EM, Cordopatis P (2007) Simulated interactions between angiotensin converting enzyme and substrate gonadotropin releasing hormone: novel insights into domain selectivity. Biochemistry 46:8753–8765
Pelmenschikov V, Blomberg MRA, Siegbahn PEM (2002) A theoretical study of the mechanism for peptide hydrolysis by thermolysin. J Biol Inorg Chem 7:284–298
Pettersen EF, Goddard TD, Huang CC, Couch GS, Greenblatt DM, Meng EC, Ferrin TE (2004) UCSF Chimera—a visualization system for exploratory research and analysis. J Comput Chem 25:1605–1612
Poger D, Mark AE (2010) On the validation of molecular dynamics simulations of saturated and *cis*-monounsaturated phosphatidylcholine lipid bilayers: a comparison with experiment. J Chem Theory Comput 6:325–336
Poger D, Gunsteren WFV, Mark AE (2010) A new force field for simulating phosphatidyl-choline bilayers. J Comput Chem 31:1117–1125
Pronk S, Páll S, Schulz R, Larsson P, Bjelkmar P, Apostolov R, Shirts MR, Smith JC, Kasson PM, Van der spoel D, Hess B, Lindahl E (2013) GROMACS 4.5: a highthroughput and highly parallel open source molecular simulation toolkit. Bioinformatics 29:845–854
Rost B, Yachdav G, Liu J (2004) The predict protein server. Nucleic Acids Res 32:321–326
Sali A, Blundell TL (1993) Comparative protein modelling by satisfaction of spatial restraints. J Mol Biol 234:779–815
Sansom CE, Hoang MV, Turner AJ (1998) Molecular modelling and site-directed mutagenesis study of endothelin converting enzyme. Protein Eng 11:1235–1241
Schulz H, Dale GE, Karimi-Nejad Y, Oefner C (2009) Structure of human endothelin-converting enzyme I complexed with phosphoramidon. J Mol Biol 385:178–187
Schweizer A, Valdenaire O, Nelbo P, Deuschle U, Dumas Milne Edwards JB, Stumpf JG, Loffler BM (1997) Human endothelin-converting enzyme (ECE-1): three isoforms with distinct subcellular localizations. Biochem J 328:871–877
Shen MY, Sali A (2006) Statistical potential for assessment and prediction of protein structures. Protein Sci 15:2507–2524
Shepherd CM, Vogel HJ (2004) A molecular dynamics study of Ca2*1*-calmodulin: evidence of interdomain coupling and structural collapse on the nanosecond timescale. Biophys J 87:780–791
Shimada K, Takahashi M, Turner AJ, Tanzawa K (1996) Rat endothelin-converting enzyme-1 forms a dimer through Cys412 with a similar catalytic mechanism and a distinct substrate binding mechanism compared with neutral endopeptidase-24.11. Biochem J 315:863–867
Spiliotopoulos D, Spitaleri A, Musco G (2012) Exploring phd fingers and h3k4me0 interactions with molecular dynamics simulations and binding free energy calculations: aire-phd1, a comparative study. PLoS One 7:e46902
Sticht H, Bayer P, Willbold D, Dames S, Hilbich C, Beyreuther K, Frank RW, Rosch P (1995) Structure of amyloid A4-(1–40)-peptide of Alzheimer's disease. Eur J Biochem 233:293–298
Takahashi M, Matsushita Y, Iijima Y, Tanzawa K (1993) Purification and characterization of endothelin-converting enzyme from rat lung. J Biol Chem 268:21394–21398
Takahashi M, Fukuda K, Shimada K, Barnes K, Turner AJ, Ikeda M, Koike M, Yamamoto Y, Tanzawa K (1995) Localization of rat endothelin-converting enzyme to vascular endothelial cells and some secretory cells. Biochem J 311:657–665
Tieleman DP, Berendsen HJC (1998) A molecular dynamics study of the pores formed by *Escherichia coli* OmpF Porin in a fully

hydrated palmitoyloleoyl phosphatidyl choline bilayer. Biophys J 74:2786–2801

Tseng GN, Sonawane KD, Korolkova YV, Zhang M, Liu J, Grishin EV, Guy HR (2007) Probing the outer mouth structure of the HERG channel with peptide toxin footprinting and molecular modeling. Biophys J 92:3524–3540

Turner AJ, Tanzawa K (1997) Mammalian membrane metallopeptidases: NEP, ECE, KELL, and PEX. FASEB J 11:355–364

Ul-Haq Z, Iqbal S, Moin ST (2012) Dynamic changes in the secondary structure of ECE-1 and XCE account for their different substrate specificities. BMC Bioinform 13:285–300

Valdenaire O, Rohrbacher E, Mattei MG (1995) Organization of the gene encoding the human endothelin-converting enzyme (ECE-1). J Biol Chem 270:29794–29798

Valdenaire O, Barret A, Schweizer A, Rohrbacher E, Françoise M, Florence P, Pierre C, Claude T (1999a) Two di-leucine-based motifs account for the different subcellular localizations of the human endothelin-converting enzyme (ECE-1) isoforms. J Cell Sci 112:3115–3125

Valdenaire O, Lepailleur-Enouf D, Egidy G, Thouard A, Barret A, Vranckx R, Tougard C, Michel JB (1999b) A fourth isoform of endothelin converting enzyme (ECE-1) is generated from an additional promoter molecular cloning and characterization. Eur J Biochem 264:341–349

Vardy ERLC, Catto AJ, Hooper NM (2005) Proteolytic mechanisms in amyloid-b metabolism: therapeutic implications for Alzheimer's disease. Trends Mol Med 11:465–472

Vorontsov II, Miyashita O (2011) Crystal molecular dynamics simulations to speed up MM/PB(GB) SA evaluation of binding free energies of di-mannose deoxy analogs with P51G-m4-Cyanovirin-N. J Comput Chem 32:1043–1053

Wallin E, Tsukihara T, Yoshikawa S, Von Heijne G, Elofsson A (1997) Architecture of helix bundle membrane proteins: an analysis of cytochrome c oxidase from bovine mitochondria. Protein Sci 6:808–815

Wiederstein M, Sippl MJ (2007) ProSA-web: interactive web service for the recognition of errors in three-dimensional structures of proteins. Nucleic Acids Res 35:407–441

Wu S, Zhang Y (2008) MUSTER: improving protein sequence profile–profile alignments by using multiple sources of structure information. Proteins 72:547–556

Xu D, Emoto N, Giaid A, Slaughter C, Kaw S, deWit D, Yanagisawa M (1994) ECE-1: a membrane-bound metalloprotease that catalyzes the proteolytic activation of big endothelin-1. Cell 78:473–485

Xu Y, Shen J, Luo X, Zhu W, Chen K, Ma J, Jiang H (2005) Conformational transition of amyloid beta-peptide. Proc Natl Acad Sci USA 102:5403–5407

Yanagisawa M, Kurihara H, Kimura S, Tomobe Y, Kobayashi M, Mitsui Y, Yazaki Y, Goto K, Masaki T (1988) A novel potent vasoconstrictor peptide produced by vascular endothelial cells. Nature 332:411–415